Journal of Metals, Materials and Minerals, Vol. 31, No. 3, pp. 47-52, 2021

Effect of zinc-hydroxo species on the growth of one-dimensional ZnO nanostructures

Nontakoch SIRIPHONGSAPAK[1] and Somyod DENCHITCHAROEN[1,*]

[1] *Department of Physics, Faculty of Science, King Mongkut's University of Technology Thonburi, Bangkok, 10140, Thailand*

***Corresponding author e-mail:** somyod.den@mail.kmutt.ac.th

Received date:
29 June 2021
Revised date
30 July 2021
Accepted date:
05 August 2021

Keywords:
Zinc-hydroxo species;
Thermodynamic simulation;
Hydrothermal growth;
1-D ZnO nanostructures

Abstract

One-dimensional ZnO nanostructures were grown on ZnO seed layer by hydrothermal method using zinc nitrate ($Zn(NO_3)_2$) and sodium hydroxide (NaOH) as precursors. The concentrations of NaOH and $Zn(NO_3)_2$ were varied from 40 mM to 680 mM and kept constant, respectively. Effects of increasing the hydroxide ions on the concentration of zinc-hydroxo species in the solution were studied using thermodynamic simulation software. The simulated results showed that $Zn(OH)_2$ and $Zn(OH)_3^-$ concentrations tended to decrease but $Zn(OH)_4^{2-}$ was non-linearly increased when the concentration of NaOH at room temperature was increased. After the growth of ZnO, the samples were characterized by FESEM and UV-vis to investigate the morphology and transmittance spectra, respectively. The results showed that the rod density of ZnO nanostructures was decreased due to lower concentrations of $Zn(OH)_2$ and $Zn(OH)_3^-$ species affecting ZnO nucleation mode. On the other hand, $Zn(OH)_4^{2-}$ was competitively higher and involved in growing 1-D ZnO nanostructures on the nucleation layer resulting in larger diameter and longer length of nanostructures. For the UV-vis results, the % transmittance spectra in visible region of grown ZnO nanostructures with NaOH concentrations from 40 to 360 mM were more than 70% but too low transmittance for 520 mM.

1. Introduction

ZnO is an impressive n-type semiconductor that has many interesting properties such as wide-direct bandgap (3.37 eV) and high exciton binding energy (60 meV). Thus, it has high thermal and chemical stability [1]. Nowadays, ZnO is downsized to nanoscale tending to increase the surface area and then used in many applications such as photocatalytic degradation [2], photoelectrochemical water splitting [3], gas sensor [4], and UV photodetector [5].

There are many methods to synthesize ZnO nanostructures such as sol-gel [6], precipitation [7], chemical vapor deposition [8], and hydrothermal method. The hydrothermal is a simple and environmentally friendly method that requires only uncomplicated equipment with an aqueous solution [9]. Generally, $Zn(NO_3)_2$ and hexamine ($(CH_2)_6N_4$) were used as precursors to obtain zinc (Zn^{2+}) and hydroxide (OH^-) ions for growing 1-D ZnO nanostructures [10-13]. The growth of ZnO nanorods is described by the chemical reactions below [9,13]:

$$(CH_2)_6N_4 + 6H_2O \rightarrow 6HCHO + 4NH_3 \quad (1)$$

$$NH_3 + H_2O \leftrightarrow NH_4^+ + OH^- \quad (2)$$

$$Zn(NO_3)_2 \rightarrow Zn^{2+} + 2NO_3^- \quad (3)$$

$$Zn^{2+} + 2HO \leftrightarrow ZnO\,(s) + H_2O \quad (4)$$

Hexamine is hydrolyzed to produce formaldehyde (HCHO) and ammonia (NH_3) which then reacts with water to have hydroxide ion (OH^-). To obtain Zn^{2+}, zinc nitrate is dissolved in water as shown in the reaction (3). Ultimately, the crystallization of ZnO (s) is formed by Zn^{2+} and OH^- ions. Not only hexamine but also alkaline media such as sodium hydroxide (NaOH) [14-16] and potassium hydroxide (KOH) [17] were used as a source of hydroxide ion for growing ZnO nanoparticles due to the precipitation caused by a higher degree of supersaturation of the solution [14].

On the other hand, there are many research groups who used alkalis for growing 1-D ZnO nanostructures on the seed layer. S. Yamabi and H. Imai [18] presented that NaOH was used to adjust the pH of the solution containing zinc ions to achieve ZnO nanocolumnar film due to a low deposition rate caused by a low level of supersaturation of solution when the concentration of zinc ions and pH were near the edge of phase stability diagram of ZnO (s) – H_2O system. R.B. Peterson *et al.* [19] showed that ZnO nanocolumns were grown on ZnO and AZO seed layers using a hot aqueous solution of zinc nitrate and NaOH with various concentrations. The length of ZnO nanostructures depended on the concentration of zinc ions in the solution that was tuned by NaOH to maintain the metastable state in the phase stability diagram. However, there are few pieces of research that reported the roles of zinc-hydroxo species on the growth of 1-D ZnO nanostructures.

In this work, zinc ion concentration was remained constant, and NaOH concentrations were varied from 40 mM to 680 mM. Thermodynamic simulation software was used to display the concentration of each zinc-hydroxo and the other inorganic species in each aqueous solution. After growing ZnO nanostructures on seed layer by hydrothermal method, morphology and optical property were investigated by FESEM and UV-vis, respectively. The relationship between the concentration of each zinc-hydroxo species and the morphology

of as-grown ZnO nanostructures was described. Moreover, the % transmittance spectra and optical bandgap were also reported.

2. Experimental

To prepare seed layer, ITO/glass substrates (10×10 mm^2) were sonicated in acetone and isopropyl alcohol. The substrates were rinsed in deionized water and dried with nitrogen gas 99.5%. Zinc acetate dihydrate and monoethanolamine were used as a precursor and a stabilizer, respectively. The concentration of the precursor is 10 mM, and the molar ratio of stabilizer to precursor is 1. Isopropyl alcohol was used as a solvent. The mixed solution was stirred at room temperature for 3 h. The homogeneous solution was then spin-coated on substrates with a rotational speed of 2500 rpm. Finally, the substrates with seed layer were annealed at 300°C to improve the crystal structure.

For growing ZnO nanostructures, the aqueous solutions containing zinc ions and hydroxide ions were prepared separately. 10 mM zinc nitrate hexahydrate was used as a source of zinc ions while hydroxide ions were dissolved from sodium hydroxide with various concentrations of 40, 200, 360, 520, and 680 mM. Each solution was stirred at room temperature for 1 h, then mixed by the volume ratio of 1:1, and stirred for 2 min before pouring into a Teflon liner stainless steel autoclave. The substrate with ZnO seed layer was placed at the bottom of the Teflon container. The autoclave was put into the oven at 90°C for 6 h. After the growth of ZnO in the autoclave, the samples with nanostructures were rinsed in DI water several times and then dried with nitrogen gas 99.5%.

Possible inorganic species in each solution with the saturation index were simulated using Visual MINTEQ version 3.1. The temperature and concentrations of $Zn(NO_3)_2$ and NaOH were added into the software. Firstly, the concentration [c] (Equation (5)) of each species was calculated from the activity {a} based on the stability constant K_i (Equation (6-7)) of each reaction (at 25°C) as shown in Table 1.

$$\{a\}_i = \gamma[c]_i \tag{5}$$

Where γ is the activity coefficient.

$$K_i = \frac{\{Zn(OH)_i^{(-i+2)+}\}}{\{Zn^{2+}\}\{OH^-\}^i} \; ; i = 1 \tag{6}$$

$$K_i = \frac{\{Zn(OH)_i^{(i-2)-}\}}{\{Zn^{2+}\}\{OH^-\}^i} \; ; i = 2, 3, 4 \tag{7}$$

Where i is the coordination number of Zn^{2+} ion and K_i is the stability constant from NIST. Secondly, the saturation index S of each solution was determined from the dissolution reaction (8) in case of i = 2, 3, 4 and the Equation (9).

Table 1. Important chemical reactions in solution and reaction constants (K) at 25°C.

Chemical reaction	log(K) (25°C)
$Zn^{2+} + OH^- \leftrightarrow Zn(OH)^+$	5.0
$Zn^{2+} + 2OH^- \leftrightarrow Zn(OH)_2$	11.1
$Zn^{2+} + 3OH^- \leftrightarrow Zn(OH)_3^-$	13.6
$Zn^{2+} + 4OH^- \leftrightarrow Zn(OH)_4^{2-}$	14.8
$Zn(OH)_2 \leftrightarrow ZnO + H_2O$	5.67
$Zn(OH)_3^- \leftrightarrow ZnO + H_2O + OH^-$	3.17
$Zn(OH)_4^{2-} \leftrightarrow ZnO + H_2O + 2OH^-$	1.97

$$ZnO + H_2O + (i-2)OH^- \leftrightarrow Zn(OH)_i^{(i-2)-} \; ; K_{sp} \tag{8}$$

$$S = \log IAP - \log K_{sp} = \log \frac{IAP}{K_{sp}} \tag{9}$$

Where IAP is the actual ion activity product and K_{sp} is the solubility product constant.

To characterize the samples, field-emission scanning electron microscope (FESEM, Hitachi S-4700) were introduced to discover the rod density from the morphology. The ultraviolet-visible spectrophotometer (UV-vis, Shimadzu UV-3101PC) was also used to study the % transmittance and optical bandgap of ZnO nanostructures.

3. Results and discussion

The morphology of 1-D ZnO nanostructures would change when the concentration of NaOH was increased from 40 mM to 680 mM as shown in Figure 1. With concentrations of 40 and 200 mM, the layer of nanostructure showed only short and dense nanorods. When the concentrations of NaOH were higher at 360, 520, and 680 mM, the morphology looked different in the way of dimension, and nanostructures were more flexible with a high aspect ratio compared to that of nanostructures at 40 and 200 mM. Moreover, the tips of each ZnO nanowire in NaOH concentration of 360, 520, and 680 mM were assembled together by nanocarpet effect [20] due to lower density of nanowires which were more flexible.

The apparent rod density of 1-D ZnO nanostructures was defined as the number of nanorods or nanowires per square micron from top-view FESEM images. The density tended to decrease when NaOH concentration was increased as shown in Figure 2 (square line). When NaOH concentration was adjusted to be 40, 200, 360, and 520 mM, the average diameters and lengths of 1-D ZnO nanostructures were 22.13, 25.22, 29.42, and 43.78 nm (Figure 2: circle line), and 142.13, 351.74, 605.76, and 2705.83 nm (Figure 2: diamond line), respectively. However, both of them could not be further increased when the concentration was over 520 mM.

The evolution of rod density, diameter, and length of the nanostructures could be explained by simulated results from Visual MINTEQ software as shown in Figure 3. Firstly, Figure 3(a) illustrated the concentrations of zinc-hydroxo species that were found in the aqueous solution before the formation of ZnO solid at 25°C. The results showed that the concentrations of $Zn(OH)_2$ and $Zn(OH)_3^-$ at 40 mM NaOH were higher than that of other zinc-hydroxo species. When the concentration of NaOH was increased, the concentration of $Zn(OH)_4^{2-}$ was also increased, but $Zn(OH)_2$ and $Zn(OH)_3^-$ concentrations were decreased. The increase of OH^-, while the concentration of Zn^{2+} is limited, causes the increase of $Zn(OH)_4^{2-}$ because the preferred coordination number for Zn^{2+} is 4 [21]. The increase of $Zn(OH)_4^{2-}$ might mainly influence the decrease of saturation index due to less equilibrium constant K for producing ZnO (s) from $Zn(OH)_4^{2-}$ comparing to the other two species as shown in the Table 1. As a result of decreasing the saturation index S, the change in Gibbs free energy ΔG for the formation of ZnO was increased as shown in the equation below [22-23]. This affected the decrease of nucleation number of ZnO nuclei leading to a lower rod density of nanostructures.

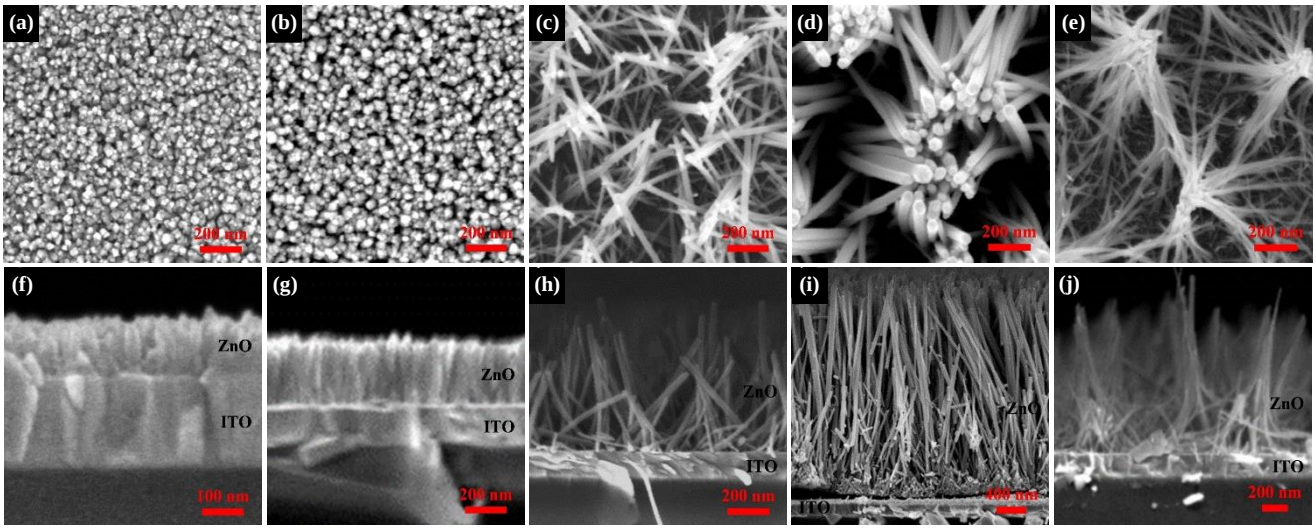

Figure 1. Top-view (a – e) and cross-sectional (f – j) FESEM images of 1-D ZnO nanostructures grown by hydrothermal method on ZnO seed layer using 10 mM $Zn(NO_3)_2$ and NaOH with various concentrations of 40 (a, f), 200 (b, g), 360 (c, h), 520 (d, i), and 680 mM (e, j).

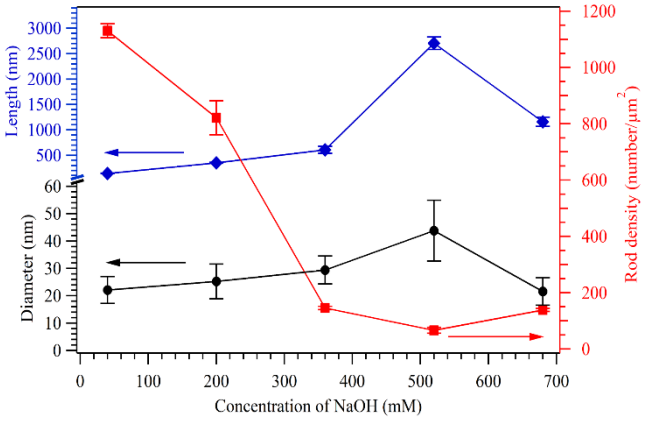

Figure 2. Average diameter, length, and apparent rod density of 1-D ZnO nanostructures grown by hydrothermal method with different concentrations of NaOH at 90°C.

$$\Delta G = -2.303\,RT \times S \quad (10)$$

Where R is the gas constant and T is the temperature. The other reason of the decreased supersaturation level and rod density might also be higher concentration of free OH^- and NaOH (aq) in solution preventing the nucleation of ZnO from $Zn(OH)_2$ and $Zn(OH)_3^-$.

Secondly, the role of $Zn(OH)_4^{2-}$ in solution on the diameter and length was confirmed by simulated results in Figure 3(d). The results presented that zinc-hydroxo species disappeared from the solution with 40 mM NaOH and became ZnO (s). When the NaOH concentration was increased, $Zn(OH)_4^{2-}$ and ZnO (s) concentrations were slightly increased and decreased, respectively. Therefore, the formation of ZnO (s) at 25°C was devoted by the portion of $Zn(OH)_4^{2-}$ and all of $Zn(OH)_2$ and $Zn(OH)_3^-$ because $Zn(OH)_4^{2-}$ was more stable than other species. Moreover, the equilibrium concentrations of zinc-hydroxo species and ZnO (s) at 90°C were shown in an inset figure in Figure 3(d). The results showed that all zinc-hydroxo species were used to form ZnO (s) at all concentrations of NaOH. Therefore, in case of higher NaOH concentration, we could confirm that $Zn(OH)_4^{2-}$ played an important role in the growth of ZnO nanostructures at 90°C.

The nucleation and growth mechanism of 1-D ZnO nanostructures could be explained by the comparison between the morphology of nanostructures and the concentrations of zinc-hydroxo species in the solution before forming ZnO (s). After the formation of zinc-hydroxo species, each species was competitive each other to form both ZnO nucleation on the seed layer and precipitation into the solution as shown in the chemical reaction (11-13) when the temperature of the solution was increased from room temperature to 90°C.

$$Zn(OH)_2 \rightarrow ZnO + H_2O \quad (11)$$

$$ZnOH_3^- \rightarrow ZnO + H_2O + OH^- \quad (12)$$

$$ZnOH_4^{2-} \rightarrow ZnO + H_2O + 2OH^- \quad (13)$$

$Zn(OH)_2$ and $Zn(OH)_3^-$ have less stable and more potential to form ZnO nuclei than $Zn(OH)_4^{2-}$. As a result, the supersaturation level of solution and rod density of ZnO were suddenly decreased with increasing NaOH concentration due to the decrease of $Zn(OH)_2$ and $Zn(OH)_3^-$ concentrations. After the nucleation process, $Zn(OH)_4^{2-}$ played an important role to further grow the nanostructure on the nucleation layer at 90°C [24]. Thus, the diameter and length of nanostructures were increased due to the increase of $Zn(OH)_4^{2-}$ concentration in solution. However, when the concentration of NaOH was increased to 680 mM, 1-D nanostructure might have more other solid phases [25], and the dimension of the nanostructure tended to be decreased.

% Transmittance spectra of 1-D ZnO nanostructures were shown in Figure 4(a). % Transmittance spectra in the visible region of all concentrations except 520 mM NaOH were higher than 70% and rapidly decreased at the wavelength of ~370 nm or below due to the absorption of ZnO. However, ZnO nanowire layer at 520 mM NaOH has very low transparency because of very high thickness, low uniformity, and low crystallinity. According to the transmittance at each wavelength, an absorption coefficient α could be calculated using the equation below [11]:

$$\alpha = (1/d)\,In(1/T) \quad (14)$$

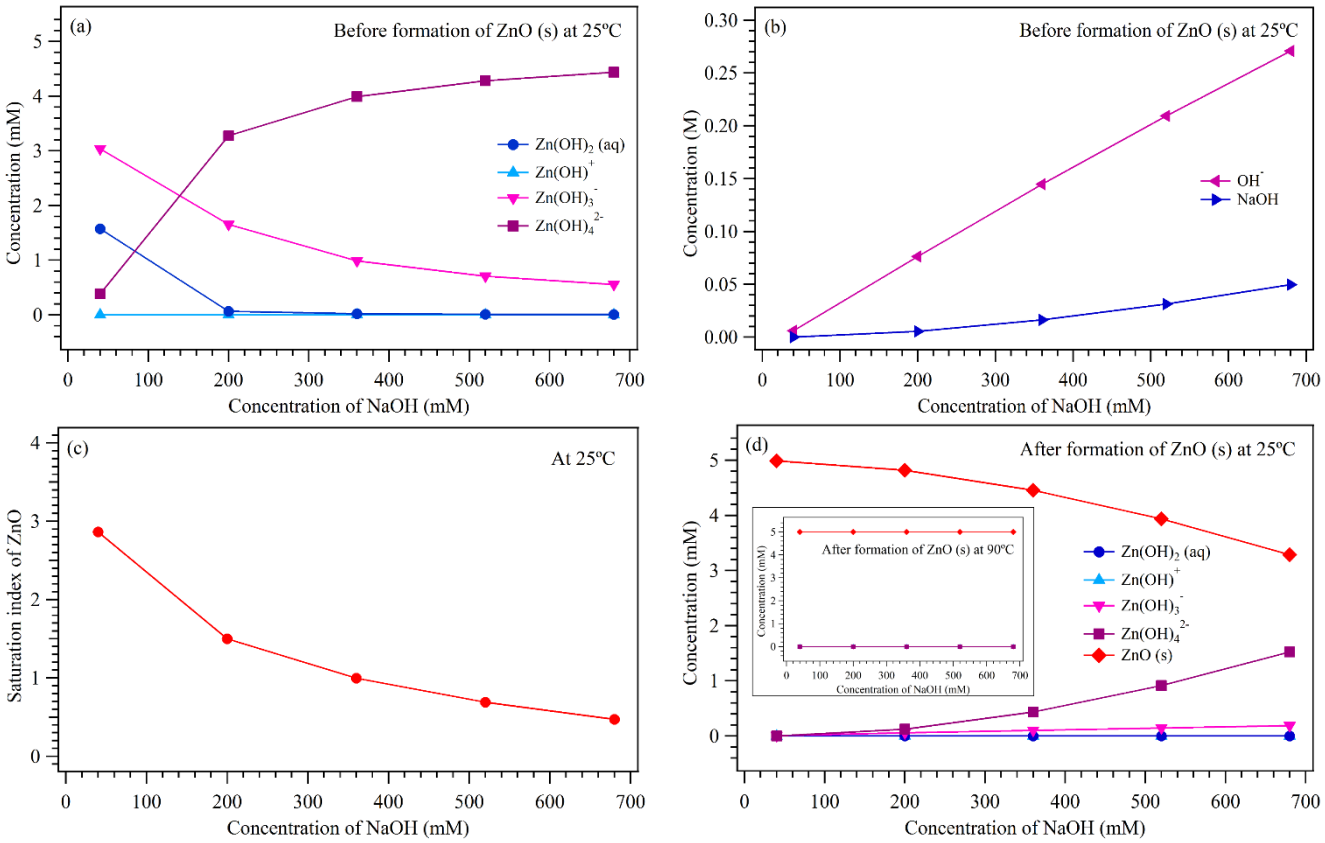

Figure 3. Concentration of (a) zinc-hydroxo species, (b) hydroxide ion and NaOH (aq) in aqueous solution, (c) saturation index of solution before forming ZnO (s) at 25°C, and (d) the concentration of zinc-hydroxo species after the formation of ZnO at 25°C and 90°C (inset) with different concentrations of NaOH simulated by using Visual MINTEQ software.

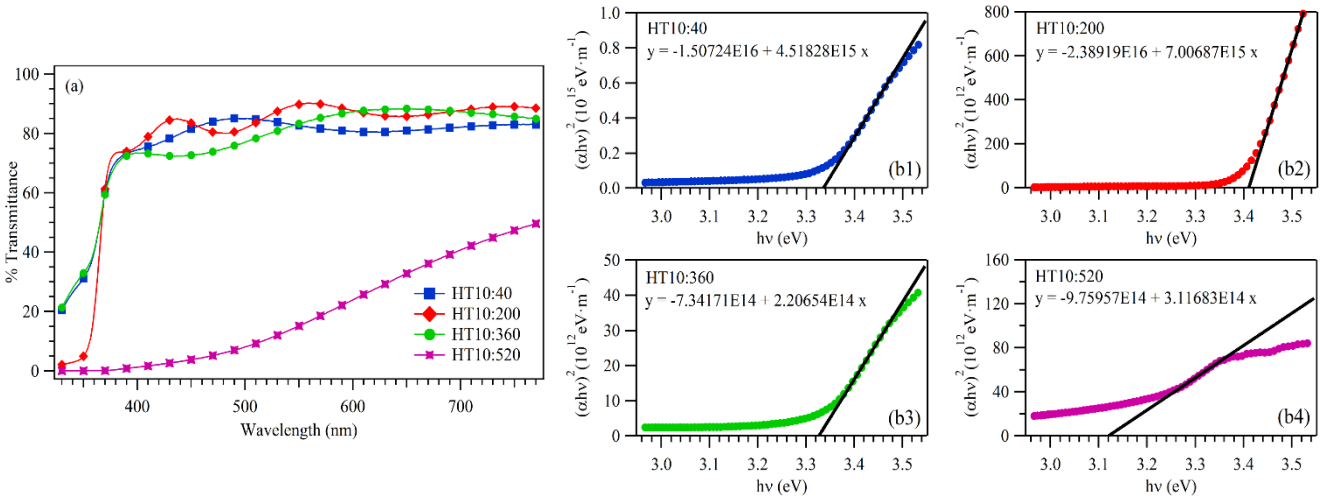

Figure 4. (a) % Transmittance spectra and (b) Tauc plot of 1-D ZnO nanostructures grown by hydrothermal method with different concentrations of NaOH.

Where T and d are the transmittance and thickness of the ZnO layer, respectively. The absorption coefficients were used to display a Tauc plot for the determination of the optical bandgap of ZnO as followed by the equation below [11]:

$$(\alpha h\nu)^{1/n} = B\left(h\nu - E_g\right) \qquad (15)$$

Where hν is the photon energy, B is the constant, E_g is the optical bandgap, and n of ZnO is 1/2 for the direct allowed band. Figure 4(b) presented the Tauc plots of 1-D ZnO nanostructures, and the optical bandgap was then determined from each concentration of NaOH. The bandgaps of ZnO at 40, 200, 360, and 520 mM NaOH are 3.336, 3.410, 3.327, and 3.131 eV, respectively as shown in Figure 5. This might be affected by larger dimension of nanostructures and stress happened inside the nanorods due to mechanical bending [26-27].

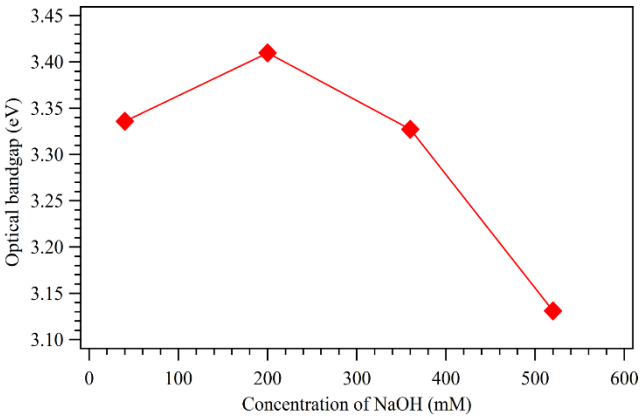

Figure 5. Optical bandgap of 1-D ZnO nanostructures grown by hydrothermal method with different concentrations of NaOH.

4. Conclusions

One-dimensional ZnO nanostructures could be grown on ZnO seed layer by hydrothermal method. The morphology of the nanostructures was changed from nanorods to be nanowires by controlling the concentration of zinc-hydroxo species in the solution that affected the nucleation and growth modes. Higher $Zn(OH)_2$ and $Zn(OH)_3^-$ at lower NaOH concentration led to higher degree of supersaturation of the solution that caused higher amount of ZnO nuclei. When NaOH concentration was increased, it resulted in the increase of $Zn(OH)_4^{2-}$ concentration leading to larger diameter and longer length of ZnO nanostructures. The optical property of the nanostructures also depended on the morphology controlled by the species in solution.

Acknowledgements

This research was financially supported by Department of Physics, Faculty of Science, King Mongkut's University of Technology Thonburi (KMUTT) and by Science Achievement Scholarship of Thailand (SAST).

References

[1] A. Janotti, and C. G. Van de Walle, "Fundamentals of zinc oxide as a semiconductor," *Reports on Progress in Physics*, vol. 72, pp. 1-29, 2009.

[2] C. Yu, Z. Tong, S. Li, and Y. Yin, "Enhancing the photocatalytic activity of ZnO using tourmaline," *Materials Letters*, vol. 240, pp. 161-164, 2019.

[3] K. Govatsi, A. Seferlis, S. G. Neophytides, and S. N. Yannopoulos, "Influence of the morphology of ZnO nanowires on the photoelectrochemical water splitting efficiency," *International Journal of Hydrogen Energy*, vol. 43, pp. 4866-4879, 2018.

[4] Q. Ma, Y. Fang, Y. Liu, J. Song, X. Fu, H. Li, S. Chu, and Y. Chen, "Facile synthesis of ZnO morphological evolution with tunable growth habits: Achieving superior gas-sensing properties of hemispherical ZnO/Au heterostructures for triethylamine," *Physica E: Low-dimensional Systems and Nanostructures*, vol. 106, pp. 180-186, 2019.

[5] N. A. Hammed, A. A. Aziz, A. I. Usman, and M. A. Qaeed, "The sonochemical synthesis of vertically aligned ZnO nanorods and their UV photodetection properties: Effect of ZnO buffer layer," *Ultrasonics – Sonochemistry*, vol. 50, pp. 172-181, 2019.

[6] M. Taheri, H. Abdizadeh, and M. R. Golobostanfard, "Formation of urchin-like ZnO nanostructures by sol-gel electrophoretic deposition for photocatalytic application," *Journal of Alloys and Compounds*, vol. 725, pp. 291-301, 2017.

[7] N. I. M. Rosli, S.-M. Lam, J.-C. Sin, and A. R. Mohamed, "Surfacetant-free precipitation synthesis, growth mechanism and photocatalytic studies of ZnO nanostructures," *Materials Letters*, vol. 160, pp. 259-262, 2015.

[8] M. Laurenti, N. Garino, S. Porro, M. Fontana, and C. Gerbaldi, "Zinc oxide nanostructures by chemical vapour deposition as anodes for Li-ion batteries," *Journal of Alloys and Compounds*, vol. 640, pp. 321-326, 2015.

[9] S. Baruah, and J. Dutta, "Hydrothermal growth of ZnO nanostructures," *Science and Technology of Advanced Materials*, vol. 10, pp. 1-18, 2009.

[10] C. Chevalier-César, M. Capochichi-Gnambodee, and Y. Leprince-Wang, "Growth mechanism studies of ZnO nanowire arrays via hydrothermal method," *Applied Physics A*, vol. 115, pp. 953-960, 2014.

[11] K. L. Foo, U. Hashim, K. Muhammad, and C. H. Voon, "Sol-gel synthesized zinc oxide nanorods and their structural and optical investigation for optoelectronic application," *Nanoscale Research Letters*, vol. 9, pp. 1-10, 2014.

[12] R. Parize, J. Garnier, O. Chaix-Pluchery, C. Verrier, E. Appert, and V. Consonni, "Effects of hexamethylenetetramine on the nucleation and radial growth of ZnO nanowires by chemical bath deposition," *The Journal of Physical Chemistry C*, vol. 120, pp. 5242-5250, 2016.

[13] L. Vayssieres, "Growth of arrayed nanorods and nanowires of ZnO from aqueous solution," *Advanced Materials*, vol. 15, pp. 464-466, 2003.

[14] Y. Zhang, and J. Mu, "Controllable synthesis of flower- and rod-like ZnO nanostructures by simply tuning the ratio sodium hydroxide to zinc acetate," *Nanotechnology*, vol. 18, pp. 1-6, 2007.

[15] R. Wahab, S. G. Ansari, Y. S. Kim, M. Song, and H.-S. Shin, "The role of pH variation on the growth of zinc oxide nanostructures," *Applied Surface Science*, vol. 255, pp. 4891-4896, 2009.

[16] P. Chand, A. Gaur, A. Kumar, and U. K. Gaur, "Effect of NaOH molar concentration on optical and ferroelectric properties of ZnO nanostructures," *Applied Surface Science*, vol. 356, pp. 438-446, 2015.

[17] A. El-Shaer, M. Abdelfatah, A. Basuni, and M. Mosaad, "Effect of KOH molarity and annealing temperature on ZnO nanostructure properties," *Chinese Journal of Physics*, vol. 56, pp. 1001-1009, 2018.

[18] S. Yamabi, and H. Imai, "Growth conditions for wurtzite zinc oxide films in aqueous solutions," *Journal of Materials Chemistry*, vol. 12, pp. 3773-3778, 2002.

[19] R. B. Peterson, C. L. Fields, and B. A. Gregg, "Epitaxial chemical deposition of ZnO nanocolumns from NaOH solutions," *Langmuir*, vol. 20, pp. 5114-5118, 2004.

[20] J.-G. Fan, D. Dyer, G. Zhang, and Y.-P. Zhao, "Nanocarpet effect: pattern formation during the wetting of vertically aligned nanorod arrays," *Nano Letters*, vol. 4, pp. 2133-2138, 2004.

[21] Z.-Q. Liu, Y. M. Ng, P. J. Tiong, R. A. A. Talip, N. Jasin, V. Y. M. Jong, and M. G. Tay, "Five-Coordinate Zinc(II) Complex: Synthesis, Characterization, Molecular Structure, and Antibacterial Activities of Bis-[*(E)*-2-hydroxy-*N'*-{1-(4-methoxyphenyl) ethylidenebenzohydrazido]dimethylsulfoxidezinc(II) Complex," International Journal of Inorganic Chemistry, vol. 2017, pp. 1-8, 2017.

[22] W. Stumm, and J. J. Morgan, *Aquatic Chemistry: Chemical Equilibria and Rates in Natural Waters*. New Yok: John Wiley & Sons, Inc., 1996.

[23] T. L. Sounart, J. Liu, J. A. Voigt, M. Huo, E. D. Spoerke, and B. McKenzie, "Secondary Nucleation and Growth of ZnO," *Journal of the American Chemical Society*, vol. 129, pp. 15786-15793, 2007.

[24] M. Wang, Y. Zhou, Y. Zhang, S. H. Hahn and E. J. Kim, "From $Zn(OH)_2$ to ZnO: a study on the mechanism of phase transformation," *CrystEngComm*, vol. 13, pp. 6024-6026, 2011.

[25] M. C. Gelabert, "Supersaturation of aqueous species and hydrothermal crystal," *Journal of Crystal Growth*, vol. 418, pp. 167-175, 2015.

[26] H. O. Chu, Q. Wang, Y. Shi, S. Song, W. Liu, S. Zhou, D. Gibson, Y. Alajlani, and C. Li, "Structural, optical properties and optical modelling of hydrothermal chemical growth derived ZnO nanowires," *Transactions of Nonferrous Metals Society of China*, vol. 30, pp. 191-199, 2020.

[27] B. Wei, K. Zheng, Y. Ji, Y. Zhang, Z. Zhang, and X. Han, "Size-Dependent Bandgap Modulation of ZnO Nanowires by Tensile Strain," *Nano Letters*, vol. 12, pp. 4595-4599, 2012.